A diffusion model for velocity gradients in turbulence

S. S. Girimaji and S. B. Pope
Sibley School of Mechanical and Aerospace Engineering, Cornell University, Ithaca, New York 14853

(Received 7 July 1989; accepted 26 October 1989)

In this paper a stochastic model for velocity gradients following fluid particles in incompressible, homogeneous, and isotropic turbulence is presented and demonstrated. The model is constructed so that the velocity gradients satisfy the incompressibility and isotropy requirements exactly. It is further constrained to yield the first few moments of the velocity gradient distribution similar to those computed from full turbulence simulations (FTS) data. The performance of the model is then compared with other computations from FTS data. The model gives good agreement of one-time statistics. While the two-time statistics of strain rate are well replicated, the two-time vorticity statistics are not as good, reflecting perhaps a certain lack of embodiment of physics in the model. The performance of the model when used to compute material element deformation is qualitatively good, with the material line-element growth rate being correct to within 5% and that of surface element correct to within 20% for the lowest Reynolds number considered. The performance of the model is uniformly good for all the Reynolds numbers considered. So it is conjectured that the model can be used even in inhomogeneous, high-Reynolds-number flows, for the study of evolution of surfaces, a problem that is of interest particularly to combustion researchers.

I. INTRODUCTION

Velocity gradients following fluid particles determine the nature of material line, surface, and volume evolution in turbulence. In combustion, the velocity gradients not only determine the growth rate of flamelet area, but also the flamelet orientation and hence the direction of propagation of the flame. Batchelor[1] has shown how the complicated general analysis of material line and surface stretching can be reduced to the analysis of infinitesimal elements over which the velocity gradients are uniform. The recent works of Yeung, Girimaji, and Pope[2] and Girimaji and Pope[3] use full turbulence simulations (FTS) data in conjunction with Batchelor's[1] equations to examine the statistics of material line and surface stretching, material volume deformation, etc. Further, Yeung, Girimaji, and Pope[2] infer the implications of their findings for flamelets in premixed combustion and constant-property scalar surfaces in diffusion flames.

Although FTS provide a means of studying important material deformation processes, they are expensive and are restricted to low-Reynolds-number turbulence. As an alternative, in their study of flamelet surfaces, Pope and Cheng[4] use velocity gradients generated from a stochastic model. Their model consists of an Uhlenbeck–Ornstein process for dissipation, and a linear combination of Gaussian stochastic processes for the normalized velocity gradients. The linear combination satisfies all constraints appropriate to homogeneous isotropic turbulence, and the scalar coefficients in the model are chosen to match correlation functions obtained from FTS data. However, the performance of the model is found to be quite poor even when some basic one-time statistics are compared with those obtained from FTS data.

The objective of the present work is to construct a model for Lagrangian velocity gradients (by Lagrangian velocity gradients we mean velocity gradients with respect to Eulerian spatial coordinates following fluid particles) that *mimic* the velocity gradients obtained from FTS. Such a model can then be used in the study of material element deformation. Since the material deformation phenomena (straining, etc.) are governed by small-scale processes, a model developed for moderate Reynolds number can be expected to be reasonably accurate even for high-Reynolds-number inhomogeneous flows.

The model developed here is a tensor-valued diffusion process for the velocity gradients. Since Taylor[5] pointed out the importance of Lagrangian velocity statistics in the analysis of turbulent diffusion, stochastic models have been used extensively (e.g., Durbin[6]) to study the problem. The stochastic model (diffusion process) time series are continuous, Markovian, and simple to compute. However, diffusion process time series are nondifferentiable: hence the autocorrelation has an exponential decay with a nonzero slope at the origin. If caution is exercised in interpreting this unphysical small-time behavior, the early proponents of diffusion model argued, the advantages offered offset the disadvantage of nondifferentiability of the model time series. This has since been accepted as a valid justification for the use of stochastic models to study diffusionlike processes.

Of late, the purview of stochastic models has been extended to inhomogeneous flows (e.g., Reid[7]), and such a model has been used as the basis for the calculation of inhomogeneous flow fields (e.g., Haworth and Pope[8]). Recently the stochastic model for Lagrangian velocity has been refined to account for internal intermittency (Pope[9]). Consideration of intermittency requires that pseudodissipation (sum of the squares of velocity gradients) following fluid particles be known and Pope[10] has suggested a lognormal Uhlenbeck–Ornstein process to model this quantity. So a stochastic model for the individual velocity gradients represents the next natural step in the progression toward further refinement.

 0899-8213/90/020242-15$02.00

The layout of the rest of the paper is as follows. In Sec. II some relevant background information on velocity gradients is provided. We justify the use of a diffusion process to model velocity gradients in Sec. III and derive the general form of the model. In Sec. IV, starting from the general form of the model, we proceed to derive the final model equation. The numerical methods used for generating sample paths, and for extracting the material-element deformation information from velocity gradients, are described in Sec. V. In Sec. VI we compare the model results with those computed from FTS data, and we also discuss the Reynolds-number dependence of the model. We conclude the paper with a brief summary and discussion of the contribution of the model.

II. BACKGROUND ON LAGRANGIAN VELOCITY GRADIENTS

At position $\mathbf{x}$ and time T, the Eulerian velocity gradients are $\partial u_i/\partial x_j(\mathbf{x},T)$. Let $\mathbf{x}^+$ denote the position, at time T, of a fluid particle. Then we denote the Lagrangian velocity gradients by

$$\frac{\partial u_i^+}{\partial x_j}(T) \equiv \frac{\partial u_i}{\partial x_j}(\mathbf{x}^+, T).$$

Here and below, the superscript $+$ indicates that the quantity is evaluated following a fluid particle. In homogeneous, isotropic turbulence, the one-point one-time statistics of $\partial u_i/\partial x_j$ and $\partial u_i^+/\partial x_j$ are identical, a fact that is exploited throughout the paper when such statistics are discussed. But the multitime statistics (e.g., temporal autocorrelations) are different for the two cases.

Let S_{ij} and R_{ij} be strain-rate tensor and rotation-rate tensor, respectively, i.e., the symmetric and the antisymmetric parts of $\partial u_i/\partial x_j$. Let a_1, a_2, and a_3 be the principal strain rates (eigenvalues of S_{ij}) with the ordering

$$a_1 \geqslant a_2 \geqslant a_3.$$

We further define dissipation ϵ, enstrophy ζ, and pseudodissipation φ as

$$\epsilon \equiv 2\nu S_{ij} S_{ij},$$

$$\zeta \equiv 2\nu R_{ij} R_{ij},$$

$$\varphi \equiv \nu \frac{\partial u_i}{\partial x_j}\frac{\partial u_i}{\partial x_j},$$

where ν is kinematic viscosity.

Under conditions of incompressibility, homogeneity, and isotropy, the velocity gradients possess the following properties:

$$\frac{\partial u_i}{\partial x_i} = 0,$$

$$\left\langle \frac{\partial u_i}{\partial x_j} \right\rangle = 0,$$

and

$$\langle \varphi \rangle = \langle \epsilon \rangle = \langle \zeta \rangle.$$

In terms of the principal strain rates, the incompressibility condition is

$$a_1 + a_2 + a_3 = 0,$$

from which it follows that

$$a_1 > 0, \quad a_3 < 0, \quad \text{and} \quad a_2 = -a_1 - a_3.$$

The sign of $\langle a_2 \rangle$ cannot be determined from these kinematic considerations alone.

FTS have shed further light on the nature of S_{ij}, R_{ij}, and about their interactions. The most important findings are listed first and then discussed briefly.

(1) The vorticity vector is preferentially aligned with the principal strain direction corresponding to the intermediate principal strain rate a_2 (Ref. 11).

(2) The intermediate principal strain rate a_2 has a positive mean value, which along with the incompressibility condition leads to a negative mean value of the invariant $S_{ij}S_{jk}S_{ki}$ (Refs. 11–13).

(3) The one-time probability density function of pseudodissipation is close to lognormal. The pdf's of dissipation and enstrophy are less so, with that of enstrophy being the farther of the two (Refs. 10 and 14).

(4) Following a fluid particle the integral time scale of enstrophy (ζ^+) is longer than that of dissipation (ϵ^+). The Lagrangian time scale of pseudodissipation (φ^+) is approximately the same as that of enstrophy (Ref. 14).

It is known from experiments that the mean of the intermediate eigenvalue of strain is positive (Monin and Yaglom[12]). Vieillefosse[13] has shown that restricted Euler equations (with gradients of strain and vorticity neglected) lead to divergence of enstrophy and dissipation in finite time: and the geometry of this divergence is such that the vorticity vector is aligned along the a_2 strain-rate direction, and that a_2 is positive. Ashurst *et al.*[11] have examined the alignment of vorticity vector with strain rate, in isotropic turbulence and homogeneous shear flow (using data obtained from 128^3 FTS). They observe that there is a high probability for the vorticity to point in the a_2 strain-rate direction and with high probability this strain rate is positive (extensive).

Yeung and Pope[14] calculated Lagrangian statistics from 128^3 FTS data of homogeneous, isotropic turbulence. They report that the integral time scales of enstrophy and pseudodissipation are longer than that of dissipation. This, they explain, may be understood by recognizing that the autocorrelations are dominated by intermittent bursts that are driven by large-scale dynamics. Enstrophy, being more intermittent, is more influenced by these large-scale bursts; leading to a longer integral time scale than dissipation.

Having provided the necessary background we now proceed to develop the model.

III. MODELING VELOCITY DERIVATIVES AS A DIFFUSION PROCESS

In this section we examine the validity of the use of a diffusion process to model velocity gradients.

Starting from the Navier–Stokes equation we can derive the following equation for the instantaneous velocity gradients:

$$\frac{\partial}{\partial T}\left(\frac{\partial u_i}{\partial x_j}\right)+u_k\frac{\partial}{\partial x_k}\left(\frac{\partial u_i}{\partial x_j}\right)$$
$$=-\frac{\partial u_k}{\partial x_j}\frac{\partial u_i}{\partial x_k}-\frac{\partial^2 p}{\partial x_i\,\partial x_j}+\nu\frac{\partial^2}{\partial x_k\,\partial x_k}\left(\frac{\partial u_i}{\partial x_j}\right), \quad (1)$$

where p is the hydrostatic pressure (divided by density). The Poisson equation for pressure obtained by contracting Eq. (1) is

$$\frac{\partial^2 p}{\partial x_i\,\partial x_i}=-\frac{\partial u_k}{\partial x_i}\frac{\partial u_i}{\partial x_k}. \quad (2)$$

Incorporating the incompressibility condition in the Navier–Stokes equation leads to the following equation for Lagrangian velocity gradients (d/dT is the rate of change following a fluid particle):

$$\frac{d}{dT}\left(\frac{\partial u_i^+}{\partial x_j}\right)+\mathscr{N}_{ij}=[\mathscr{P}_{ij}+\mathscr{V}_{ij}](\mathbf{x}^+,T), \quad (3)$$

where

$$\mathscr{N}_{ij}=\left(\frac{\partial u_k^+}{\partial x_j}\right)\left(\frac{\partial u_i^+}{\partial x_k}\right)-\frac{1}{3}\delta_{ij}\left(\frac{\partial u_l^+}{\partial x_m}\right)\left(\frac{\partial u_m^+}{\partial x_l}\right),$$
$$\mathscr{P}_{ij}=-\left(\frac{\partial^2 p}{\partial x_i\,\partial x_j}-\frac{1}{3}\delta_{ij}\frac{\partial^2 p}{\partial x_m\,\partial x_m}\right),$$

and

$$\mathscr{V}_{ij}=\nu\frac{\partial^2}{\partial x_k\,\partial x_k}\left(\frac{\partial u_i}{\partial x_j}\right).$$

The terms on the right-hand side (the anisotropic-pressure term $\mathscr{P}_{ij}$ and the viscous term $\mathscr{V}_{ij}$, respectively) are evaluated at the Eulerian coordinate $\mathbf{x}^+$ at time T. The left-hand side of Eq. (3) appears in closed form in terms of the Lagrangian velocity gradient. However, the anisotropic-pressure term depends globally and the viscous term locally on the Eulerian velocity gradient field.

Vieillefosse[13] analytically investigated the interaction between the Eulerian strain rate and vorticity using the following simplified model:

$$\frac{\partial}{\partial T}\left(\frac{\partial u_i^+}{\partial x_j}\right)=-\mathscr{N}_{ij}, \quad (4)$$

where the gradients of strain rate and vorticity, $\mathscr{P}_{ij}$ and $\mathscr{V}_{ij}$, have been neglected. The incompressibility condition further simplifies the model to only eight first-order differential equations for which Vieillefosse obtains asymptotic solutions. This simple model explains some important velocity-gradient dynamics such as the small positive value of the intermediate eigenvalue of strain rate and the propensity of the vorticity vector to point along the eigenvector associated with this intermediate eigenvalue. However, because of the neglect of $\mathscr{P}$ and $\mathscr{V}$ the strain rate and vorticity of this model diverge in finite time.

Our object then is to model the anisotropic-pressure term $\mathscr{P}_{ij}$ and the viscous term $\mathscr{V}_{ij}$ in the exact equation [Eq. (3)], while retaining intact the nonlinear term $\mathscr{N}_{ij}$. By retaining $\mathscr{N}_{ij}$ in its exact form, we remove the onus on the model terms to simulate the physics already contained in this term. Since we are interested in the Lagrangian velocity gradient, the advection term is contained in the time gradient and hence need not be modeled. We model $(\partial u_i^+/\partial x_j)(T)$ as a Markov process. (The Markov process is a process where the increment in time of the process variable depends on the past only through the present. In other words the increment does not include any time-dependent integrals of the process variable.) This implies that $\mathscr{P}_{ij}$ and $\mathscr{V}_{ij}$ are modeled as stochastic functions of $\partial u_i^+/\partial x_j$. Specifically, $\partial u_i^+/\partial x_j$ is modeled as a diffusion process, which is the only Markov process with continuous sample paths. Apart from the continuity of the sample paths, the choice of a diffusion process is motivated by its computational simplicity and its success in modeling fluid particle velocity in turbulence (e.g., Haworth and Pope[8] and Durbin[6]).

The time series of a diffusion process, however, is not differentiable. The use of a diffusion process to model any continuous process is justified if it can be shown that the frequencies (or the time scales) that the diffusion model cannot simulate are dynamically unimportant. (Dynamically important scales are those scales that contain most of the power in the frequency spectrum.) For the case of velocity in high-Reynolds-number turbulence the justification is provided by the Kolmogorov 1941 hypotheses (Obukhov[15]). At high-Reynolds numbers there is a separation of the energy-containing large scales and the dissipative small scales. The Kolmogorov 1941 hypotheses state that in the inertial subrange (whose scales are much smaller than the dynamically important large scales but larger than the dissipative scales), $\langle\epsilon\rangle$ is the only parameter of relevance. This implies that the frequency spectrum in the inertial range is inversely proportional to the square of the frequency. In the small-scale range the velocity frequency spectrum of turbulence decreases faster than any negative power of the frequency. In the small-scale range, the frequency spectrum from a diffusion process, however, is inversely proportional to the square of the frequency. So the diffusion model can simulate large scales and the inertial-range scales adequately though not the small scales. Since for velocity only the large scales are dynamically important, the diffusion process can be used to model this quantity. Such a simple justification is not possible for the case of velocity gradients.

The entire frequency spectrum of the velocity gradients is contained within the small-scale range of frequencies. It is important to note that the small scales are so called because they are small compared to the kinetic energy containing scales in turbulence. Indeed these *small scales* contain the entire range of large–small scales of the velocity-gradient frequency spectrum. We will refer to the various ranges of this spectrum as the viscous-large scales, viscous-intermediate scales, and viscous-small scales. It is this Lagrangian velocity-gradient frequency spectrum that is of relevance in the examination of the amenability of velocity gradient to a diffusion process.

For the lack of any hypothesis about the structure of the Lagrangian velocity-gradient frequency spectrum we appeal to the FTS data. In Fig. 1(a) we present a log–log plot of the velocity gradient (of the $\partial u_1/\partial x_1$ component) frequency spectrum along with its tangent of slope -2 for the $R_\lambda = 90$ case. In the plot provided, both velocity gradients and time are normalized by the Kolmogorov time scale

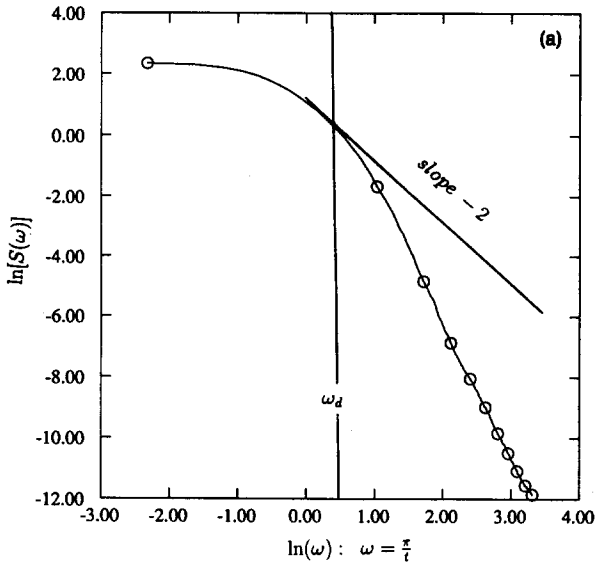

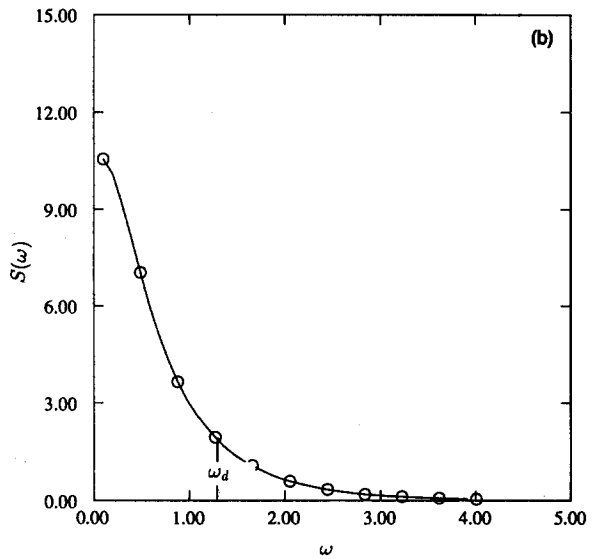

FIG. 1. Lagrangian velocity-derivative frequency spectrum: The spectrum plotted is of $(\partial u_1/\partial x_1)\tau_\eta$. The ordinate is $\omega = (\pi/T)\tau_\eta$. (a) $\ln S(\omega)$ vs $\ln \omega$. The solid line corresponds the tangent of slope -2. (b) $S(\omega)$ vs ω.

$\tau_\eta\,[=(\nu/\langle\epsilon\rangle)^{1/2}]$. We define the diffusion frequency (ω_d) as the frequency at which the line of slope -2 is tangent to the spectrum. For frequencies larger than the diffusion frequency, the frequency spectrum of a diffusion process would follow the tangent rather than the curve indicating that these scales will not be simulated well. The diffusion time scale (π/ω_d) is about $2.3\tau_\eta$. In Fig. 1(b) the frequency spectrum is presented on a linear scale. About 80% of the power is contained in scales larger than $3\,\tau_\eta$. The power contained in scales smaller than $2.3\tau_\eta$ is only about 15%. The power content of scales smaller than the Kolmogorov time scale is negligible. Hence the use of a diffusion process to model velocity gradients is justified with the understanding that the scales of about the order of Kolmogorov scale are inaccurately described.

A. General form of the model

Let h_{ij} be the normalized velocity gradient following a fluid particle and t the normalized time, such that

$$h_{ij}(t) \equiv \frac{\partial u_i^+}{\partial x_j}(T)\tau_\eta, \qquad t \equiv T/\tau_\eta, \tag{5}$$

where T is regular time. The normalized nonlinear, anisotropic-pressure, and viscous terms are

$$N_{ij} \equiv \mathcal{N}_{ij}\tau_\eta^2, \quad P_{ij} \equiv \mathcal{P}_{ij}\tau_\eta^2, \quad V_{ij} \equiv \mathcal{V}_{ij}\tau_\eta^2. \tag{6}$$

Let s_{ij}^+ and r_{ij}^+ be the symmetric and antisymmetric parts of h_{ij},

$$s_{ij}^+ = \tfrac{1}{2}(h_{ij} + h_{ji}), \qquad r_{ij}^+ = \tfrac{1}{2}(h_{ij} - h_{ji}).$$

We seek to model the evolution of h_{ij} by a diffusion process of the general form,

$$dh_{ij} \equiv h_{ij}(t + dt) - h_{ij}(t) = [-N_{ij} + M_{ij}]dt + D_{ijkl}\,dW_{kl}, \tag{7}$$

where [M–N] and **D** are the drift and diffusion coefficients, respectively, which depend (in a way to be determined) on $\mathbf{h}(t)$. Note that W_{kl} is a tensor-valued isotropic Wiener process, whose components are such that

$$\langle dW_{kl}\rangle = 0$$

and

$$\langle dW_{pq}\,dW_{kl}\rangle = \delta_{pk}\delta_{ql}\,dt.$$

B. Equations for the joint pdf of velocity gradient

Let $f(\mathbf{h};t)$ and $f_m(\mathbf{h};t)$ be the joint pdf's of the Lagrangian velocity gradients calculated from the Navier–Stokes equation [Eq.(3)] and the model [Eq.(7)], respectively. Their evolution equations are (Karlin and Taylor[16])

$$\frac{df}{dt} = -\frac{\partial}{\partial h_{ij}}[f(P_{ij} + V_{ij} - N_{ij})] \tag{8}$$

and

$$\frac{df_m}{dt} = -\frac{\partial}{\partial h_{ij}}[f_m(M_{ij} - N_{ij})] + \frac{1}{2}\frac{\partial^2}{\partial h_{kl}\,\partial h_{pq}}[D_{ijkl}D_{ijpq}f_m]. \tag{9}$$

Comparing the above two equations it can be seen that Eq. (7) provides a closure model for the joint pdf equation, Eq. (8).

The diffusion model [Eq. (7)] leads to a valid evolution of $f_m(\mathbf{h};t)$. Given appropriate initial and boundary conditions, the diffusion model with any finite **M** leads to a realizable f_m and hence all the moments of **h** are also realizable (Pope[17]). Further, for any given f, there exists a combination of **M** and **D** for which $f_m = f$ (Pope[18]). However, it is difficult to specify f completely and determine the corresponding **M** and **D**. Instead we specify only the first few moments. A diffusion model is called consistent to order n if

the moments of f_m up to order n are equal to those of f. In our case we obtain the moments of f from FTS data.

In this section we have justified the use of a diffusion process to model velocity gradients. The nonlinear term **N**, which explains many important dynamics of the velocity gradients, is retained in its exact form in the model. The modeled multitime statistics cannot be correct for small time intervals; but they can be for intervals greater than $2.3\tau_\eta$, and these time scales contain about 85% of the power. We have also established the existence of model parameters **M** and **D**, which will lead to the model one-time velocity-gradient joint pdf to be identical to that from Navier–Stokes equation. We now proceed to determine these parameters.

IV. DETERMINATION OF MODEL PARAMETERS

The object of this section is to construct the specific forms of **M** and **D** that result in the time series of h_{ij} possessing properties similar to those of FTS time series. In the case of the diffusion model for velocity, the Kolmogorov 1941 hypotheses is used to specify the diffusion term to within a constant. Consistency constraints are then imposed to determine the drift terms. In the case of a diffusion model for velocity gradients, however, no such specification of the diffusion term is possible. The three types of constraints used to construct **M** and **D** are (1) kinematic constraints; (2) lognormality of the model pseudodissipation; and (3) moment constraints.

A. Kinematic constraints

The kinematic properties of the model velocity gradients must be consistent with the velocity-gradient properties discussed in Sec. II. The choice of **M** and **D** should lead to the incompressibility condition being satisfied exactly and the conditions of homogeneity and isotropy to within statistical error. Referring to Sec. II we can write down the following kinematic properties of h_{ij}:

$$h_{ii} = 0, \quad \langle h_{ij} \rangle = 0,$$
$$h_{ij}h_{ij} = \varphi^* = \varphi^+ \langle \varphi \rangle, \quad \langle h_{ij}h_{ij} \rangle = 1,$$
$$\langle s_{ij}^+ s_{ij}^+ \rangle = \langle r_{ij}^+ r_{ij}^+ \rangle = \tfrac{1}{2}.$$

From Eq. (7) it is clear that incompressibility condition is satisfied if (note that $N_{ii} = 0$)

$$M_{ii} = 0, \quad D_{iikl} = 0.$$

The isotropy condition requires that **M** and **D** be isotropic tensor functions and that the expectations of velocity gradients be zero. Taking the expectation of Eq. (7) yields

$$\langle dh_{ij} \rangle = \langle M_{ij} - N_{ij} \rangle dt + \langle D_{ijkl} \rangle \langle dW_{kl} \rangle. \tag{10}$$

The Wiener process is independent of **D** and has an expected value of zero, leaving only the mean of the drift term. Since **M** is an isotropic tensor function,

$$\langle M_{ij}(t) - N_{ij}(t) \rangle = \langle M_{ll}(t) - N_{ll}(t) \rangle \delta_{ij}/3$$
$$= 0 \text{ (due to continuity).}$$

So if the initial velocity gradient field is isotropic (that is, $\langle h_{ij}(0) \rangle = 0$) and **M** and **D** are isotropic functions of **h**, Eq. (10) implies that the continuity condition alone ensures isotropy at later times.

The fulfillment of the homogeneity constraint, that the expected values of enstrophy and dissipation be the same, is discussed later (Sec. IV C).

B. Lognormality of pseudodissipation

It has long been conjectured that the one-time probability density function of φ is lognormal.[12] Pope[10] has noted that the FTS data of Yeung *et al.*[14] indeed confirm the conjecture and, moreover, $\ln \varphi^+$ time increments are close to Gaussian. Based on these observations he has suggested a lognormal Uhlenbeck–Ornstein (UO) process to model φ^+, with the variance (σ^2) and the time scale ratio (τ) of $\ln \varphi^+$ as the only parameters. The time scale ratio τ is the ratio between the integral time scale (τ_i) and the Kolmogorov time scale (τ_η).

The UO process suggested by Pope[10] to model pseudodissipation is

$$d\varphi^* = \varphi^* dt(\hat{a}^2 - \ln \varphi^*/\tau) + (2\hat{a}\varphi^*)dW, \tag{11}$$

where

$$\hat{a}^2 \equiv \sigma^2/2\tau$$

and dW is the increment of a Wiener process. The pseudodissipation and time in the model have been normalized with τ_η.

We impose the lognormality constraint by requiring that the φ^* process implied by Eq. (7) be identical to Pope's[10] lognormal model [Eq. (11)], which has been found to match the FTS data well. From Eq. (7) the diffusion process for φ^* is

$$d\varphi^* = dt\,[2h_{ij}(M_{ij} - N_{ij}) + D_{ijkl}D_{ijkl}] + 2h_{ij}D_{ijkl}\,dW_{kl}. \tag{12}$$

In Appendix A the conditions to be satisfied by **M** and **D** to make Eqs. (12) and (11) equivalent are considered. It is shown that with a simple model

$$D_{ijkl} = \hat{a}\sqrt{\varphi^*}(\delta_{ik}\delta_{jl} - \tfrac{1}{3}\delta_{ij}\delta_{kl}), \tag{13}$$

the diffusion terms are equivalent. With this choice a general model for the drift term is

$$M_{ij} = -h_{ij}\left(\frac{7}{2}\hat{a}^2 + \frac{\ln \varphi^*}{2\tau} - \frac{h_{lm}N_{lm}}{\varphi^*}\right) + L_{ij}, \tag{14}$$

where L_{ij} is an arbitrary isotropic tensor-valued function that satisfies

$$h_{ij}L_{ij} = 0, \quad L_{ii} = 0. \tag{15}$$

This choice of **M** and **D** satisfies continuity and hence isotropy constraints as well.

So, the complete model can be written as

$$dh_{ij} = -N_{ij}\,dt - h_{ij}\left(\frac{7}{2}\hat{a}^2 + \frac{\ln \varphi^*}{2\tau} - \frac{h_{lm}N_{lm}}{\varphi^*}\right)dt + L_{ij}\,dt + D_{ijkl}\,dW_{kl}. \tag{16}$$

It is important to note that φ^* is a lognormal process independent of the choice of **L**, provided only that Eq. (15) is satisfied. The specification of **L**, however, plays an important role in influencing other invariants of **h** and is the subject of the next subsection.

TABLE I. Complete set of isotropic functions.

List of scalars	
$I = \mathrm{tr}\,\mathbf{ss}$	$IV = \mathrm{tr}\,\mathbf{srr}$
$II = \mathrm{tr}\,\mathbf{sss}$	$V = \mathrm{tr}\,\mathbf{ssrr}$
$III = -\mathrm{tr}\,\mathbf{rr}$	$VI = \mathrm{tr}\,\mathbf{ssrrsr}$

List of symmetric tensors	
$\mathbf{F}^1 = \mathbf{J}$	$\mathbf{F}^5 = \mathbf{sr} - \mathbf{rs}$
$\mathbf{F}^2 = \mathbf{s}$	$\mathbf{F}^6 = \mathbf{rsr}$
$\mathbf{F}^3 = \mathbf{ss}$	$\mathbf{F}^7 = \mathbf{ssr} - \mathbf{rss}$
$\mathbf{F}^4 = \mathbf{rr}$	$\mathbf{F}^8 = \mathbf{rsrr} - \mathbf{rrsr}$

List of antisymmetric tensors
$\mathbf{F}^9 = \mathbf{r}$
$\mathbf{F}^{10} = \mathbf{sr} + \mathbf{rs}$
$\mathbf{F}^{11} = \mathbf{srr} - \mathbf{rrs}$

C. Modeling L to yield correct moments

As mentioned in the previous section, there exists an $\mathbf{L}$ that leads to $f_m(\mathbf{h};t) = f(\mathbf{h};t)$ (Pope[18]). But this exact $\mathbf{L}$ is difficult to determine for two reasons: the exact specification of f is difficult; and, even if it is specified correctly, there is no established procedure to determine the corresponding $\mathbf{L}$. In this subsection we devise a procedure to determine an $\mathbf{L}$ that leads to a fourth-order consistent model.

For the velocity gradients generated by Eq. (16) to be considered a good facsimile of the FTS data, we require that some higher-order moments of s^+ and $\mathbf{r}^+$, as well as some basic cross-covariances of the model, be approximately the same as those of FTS data. In particular, we consider that (refer to Table I for nomenclature) $\langle \mathrm{I} \rangle$, $\langle \mathrm{II} \rangle$, $\langle \ln(\mathrm{I}) \rangle$, $\langle \mathrm{III} \rangle$, $\langle \ln(\mathrm{III}) \rangle$, $\langle \mathrm{IV} \rangle$, $\langle \mathrm{V} \rangle$, $\langle \mathrm{IV}/(\sqrt{\mathrm{I}}\,\mathrm{III}) \rangle$, and $\langle s_{ij}^+ r_{jk}^+ s_{kl}^+ r_{li}^+ / (\mathrm{I}\,\mathrm{III}) \rangle$ are important invariants and should be reproduced well by the model. The first three constrain the model pdf of $\mathbf{s}^+$, the next two restrict the pdf of $\mathbf{r}^+$, and the rest ensure correct correlation between $\mathbf{s}^+$ and $\mathbf{r}^+$. The last two invariants have a direct bearing on the orientation of vorticity vector with respect to the principal strain directions. The homogeneity condition is satisfied by constraining only one of $\langle \mathrm{I} \rangle$ and $\langle \mathrm{III} \rangle$, since their sum $\langle \varphi^* \rangle$ is already suitably constrained.

1. General form of L

The tensor $\mathbf{L}$ is to be modeled with isotropic scalar-valued and tensor-valued functions of $\mathbf{h}$. We do not include the fluid particle velocity $\mathbf{u}$ in the model for the tensor $\mathbf{L}$ for the following reasons: inclusion of any mean velocity leads to a violation of the Galilean invariance principle; and Kolmogorov (1941 and 1962) hypotheses preclude any influence of large scales (such as fluctuating velocity) over small scales (such as velocity gradients).

We appeal to representation theorems to provide a complete, irreducible (linearly independent) set of scalars and tensors of $\mathbf{h}$. Pennisi and Trovato[19] provide such a set that is listed in Table I. There are six scalars I–VI and 11 tensor functions $\mathbf{F}^1$–$\mathbf{F}^{11}$. Any isotropic function of $\mathbf{h}$ can be expressed as a linear combination of the $\mathbf{F}$'s with coefficients depending on the scalars and constants.

In order to satisfy Eq. (15) identically, we replace the set of tensor functions $\{\mathbf{F}^\alpha\}$ with the modified set $\{\mathbf{X}^\alpha\}$:

$$\mathbf{X}^\alpha = \mathbf{F}^\alpha - \tfrac{1}{3}\mathbf{J}F_{ii}^\alpha - \mathbf{h}(F_{lm}^\alpha h_{lm}/h_{pq}h_{pq}) \tag{17}$$

($\mathbf{J}$ is the identity matrix). Since the tensors $\{\mathbf{X}^\alpha\}$ satisfy

$$X_{ii}^\alpha = 0, \quad h_{ij}X_{ij}^\alpha = 0,$$

they can be used without further constraint to construct $\mathbf{L}$. It turns out from the above definition that $\mathbf{X}^1 \equiv 0$ and $\mathbf{X}^2 \equiv \mathbf{X}^9$. In terms of $\{\mathbf{X}^\alpha\}$, the general form of $\mathbf{L}$ is

$$\mathbf{L} = \sum_{\alpha=1}^{\Lambda} \sum_{\beta=1}^{11} C_{\alpha\beta}\Gamma_\alpha \mathbf{X}^\beta, \tag{18}$$

where Γ_α are specified scalar functions, Λ is the number of scalar functions considered, and $C_{\alpha\beta}$ are constants. For the most general representation Λ is infinite, but here for practical reasons we restrict ourselves to finite Λ.

2. Determination of $\{\Gamma_\alpha\}$ and C

The determination of an optimum combination of $\{\Gamma_\alpha\}$ and $\mathbf{C}$ is considered next. An optimum combination is defined loosely as that set $\{\Gamma_\alpha\}$, which yields desired values of the moments with the least number of nonzero $\mathbf{C}$ components. To achieve this end we adopt the following strategy.

(1) Pleading simplicity we consider only tensors of up to second-order multiples of $\mathbf{h}$, and hence drop $\mathbf{X}^6$, $\mathbf{X}^7$, $\mathbf{X}^8$, and $\mathbf{X}^{11}$ from further consideration. In other words, we permit nonzero values of $C_{\alpha\beta}$ only for $\beta = 2, 3, 4, 5$, or 10.

(2) The evolution equations for the moments are derived in terms of $\mathbf{h}$, $\mathbf{D}$, and $\mathbf{L}$ (presented in Appendix B). These equations give an idea of the scalar functions that affect the values of these moments directly and thus suggest a good guess for the scalar function set $\{\Gamma_\alpha\}$. After some experimentation the two scalar functions chosen are

$$\Gamma_1 = p \equiv \sqrt{\mathrm{I}/\mathrm{III}}, \quad \Gamma_2 = 1/p.$$

(3) Once the choice of the scalar functions is made, the evolution equations of the moments $\langle \mathrm{I} \rangle$, $\langle \mathrm{II} \rangle$, $\langle \ln \mathrm{III} \rangle$, and $\langle \mathrm{IV}/(\sqrt{\mathrm{I}}\,\mathrm{III}) \rangle$ are posed as constraints to determine the constant tensor $\mathbf{C}$ (using the method described in detail in Appendix B). Nonzero values of $C_{\alpha\beta}$ are permitted only for $\beta = 3, 4$, or 10, since it is found that the optimum values of the constants for the other β's are close to zero anyway. The chosen scalar set $\{\Gamma\}$ and the constant tensor $\mathbf{C}$ are such that they cause the steady-state moments of the model to take prescribed values. These desired values are computed from FTS data.

Following the *modus operandi* explained above, using the $R_\lambda = 38$ FTS data of Yeung *et al.*[20] to prescribe values of various moments, we arrive upon the following equation for $\mathbf{h}$:

$$dh_{ij} = \Big[-\Big(N_{ij} - h_{ij}\frac{h_{lm}N_{lm}}{\varphi^*}\Big) - h_{ij}\Big(\frac{7}{2}\hat{a}^2 + \frac{\ln\varphi^* C_{24}}{2\tau}\Big) - C_{13}pX^3_{ij} - \Big(C_{14}p - \frac{\ln\varphi^* C_{24}}{p}\Big)X^4_{ij} - C_{1,10}pX^{10}_{ij}\Big]\times dt + D_{ijkl}\,dW_{kl}, \tag{19}$$

where

$C_{13} = 0.700$, $C_{14} = 1.019$,
$C_{24} = 0.307$, $C_{1,10} = 1.271$,

with other C's being zero and

$$X^3_{ij} = (s^+_{ik}s^+_{kj} - s^+_{ij}\,\mathrm{II}/\varphi^* - \delta_{ij}\mathrm{I}/3) - r^+_{ij}\,\mathrm{II}/\varphi^*,$$
$$X^4_{ij} = (r^+_{ik}r^+_{kj} - s^+_{ij}\,\mathrm{IV}/\varphi^* + \delta_{ij}\mathrm{III}/3) - r^+_{ij}\,\mathrm{IV}/\varphi^*,$$
$$X^{10}_{ij} = 2(s^+_{ij}\,\mathrm{IV}/\varphi^*) + (s^+_{ik}r^+_{kj} + r^+_{ik}s^+_{kj} + 2r^+_{ij}\,\mathrm{IV}/\varphi^*).$$

An important point to be noted is the fact that the L and N terms are of order φ^* whereas the remainder of the drift terms are of the order $\sqrt{\varphi^*}$ and $\sqrt{\varphi^*}\ln\varphi^*$. So at high values of φ^* the L and N terms play a more important role in determining the evolution of the velocity gradient. Hence it is possible to have very rapid changes in the individual velocity gradients without φ^* changing much. The realizability of the moments of the model is guaranteed for any finite L (Pope[17]). Some terms in the model equation [Eq. (19)], however, are inversely proportional to $\sqrt{\mathrm{I}}$ and $\sqrt{\mathrm{III}}$ raising the question if the model is realizable in the limit of these quantities tending to zero. It is shown in Appendix C that the model is realizable at these limits.

Since velocity gradients are small-scale quantities, this model (matched for $R_\lambda \approx 38$) can be expected to be reasonably accurate even for higher Reynolds numbers, provided the values of σ^2 and τ corresponding to that Reynolds number are used. Empirical expressions for $\sigma^2(R_\lambda)$ and $\tau(R_\lambda)$ determined from FTS data provided in Yeung and Pope[14] can be used for this purpose. To substantiate this conjecture we study the Reynolds number dependence of the model in Sec. VI.

D. Equation for unnormalized velocity gradients

So far we have concerned ourselves with stationary, homogeneous, isotropic turbulence. Most flows of practical interests are, however, nonstationary and inhomogeneous with the Eulerian pseudodissipation following a fluid particle ($\langle\varphi\rangle^+$) varying in space and time. In such flows the increments of the velocity gradients [see Eq. (5)] also include the change in the Kolmogorov time scale. Although the model is tuned to mimic low-Reynolds-number turbulence, the *universality* of the small scales, we conjecture, will permit the use of this model for inhomogeneous high-Reynolds-number turbulence. For applications to these flows, it may be convenient to write the stochastic model in terms of unnormalized quantities.

First we redefine the Kolmogorov time scale following the fluid particle to be

$$\tau^+_\eta(T) = [\nu/\langle\varphi\rangle^+]^{1/2}.$$

If local isotropy prevails, then this reverts to the standard definition (since then we have $\langle\epsilon\rangle = \langle\varphi\rangle$). The increment in regular time following the fluid particle is

$$d_T\tau^+_\eta(T) \equiv \tau^+_\eta(T + dT) - \tau^+_\eta(T) = -\tfrac{1}{2}\tau^+_\eta(T)\,d_T\ln\langle\varphi\rangle^+,$$

(assuming ν to be constant). Using this result and standard transformation rules, we obtain from Eqs. (11) and (5)

$$d_T\frac{\partial u_i^+}{\partial x_j}(T) = (M_{ij} - N_{ij})\frac{dT}{\tau^{+2}_\eta} + \frac{D_{ijkl}\,d\overline{W}_{kl}}{\tau^{+3/2}_\eta} + \frac{1}{2}\frac{\partial u_i^+}{\partial x_j}d_T\ln\langle\varphi\rangle^+. \tag{20}$$

Here $\overline{W}_{kl}$ is a Wiener process in regular time, such that

$$\langle d\overline{W}_{ij}\,d\overline{W}_{kl}\rangle = dT\,\delta_{ik}\delta_{jl}.$$

The model for **D** is given by Eq. (13), while that of M_{ij} can be identified from Eq. (19). If the mean pseudodissipation field is known—perhaps from standard model equations for dissipation—then the increment in Eq. (20) can be determined by

$$d_T\ln\langle\varphi\rangle^+ = \frac{dT}{\langle\varphi\rangle}\Big(\frac{\partial\langle\varphi\rangle}{\partial t} + \mathbf{u}^+\cdot\nabla\langle\varphi\rangle\Big).$$

V. NUMERICAL METHOD

To test the model, we generate velocity-gradient time series from Eq. (19), extract various statistics of interest, and compare the values with those obtained from FTS. The material element deformation quantities of interest that are compared to assess the model are the length vector (**l**) of the line elements; the area vector (**A**) described by two initially orthogonal material line elements; the Cauchy–Green tensor (**W**) of a triplet of initially orthogonal material lines; the angle (θ) between two material lines that are initially orthogonal; and the angle (α) between the normal to a material plane and a material line, which is initially normal. Two other quantities of interest are the angle (Γ_l) between a material line element and the instantaneous maximum positive principal strain-rate direction; and the angle (Γ_A) between the area normal of a material element and the instantaneous maximum compressive principal strain-rate direction. If $\mathbf{l}^1$, $\mathbf{l}^2$, and $\mathbf{l}^3$ are three initially orthogonal material line elements following each particle, the other quantities of interest can be calculated using the following simple trigonometric relationships:

$$\mathbf{A}(t) = \mathbf{l}^1\times\mathbf{l}^2, \quad \mathbf{W}(t) = \mathbf{U}\mathbf{U}^{\mathrm{T}}$$
$$\cos\theta = \mathbf{l}^1\cdot\mathbf{l}^2/(|\mathbf{l}^1||\mathbf{l}^2|), \quad \cos\alpha = \mathbf{A}\cdot\mathbf{l}^3/(|\mathbf{A}||\mathbf{l}^3|), \quad \cos\Gamma_l = \mathbf{l}^1\cdot\mathbf{P}/|\mathbf{l}^1|, \quad \cos\Gamma_A = \mathbf{A}\cdot\mathbf{N}/|\mathbf{A}|. \tag{21}$$

In the above equations **P** and **N** are unit vectors in the a_1 and a_3 strain-rate directions, respectively. The tensor **U** is defined by Eq. (22).

In this section we discuss the numerical procedures used: to generate sample paths of velocity gradients; and to extract the material element deformation statistics from the velocity gradients. In our calculations we generate 4000 sample paths of **h** by numerically solving Eq. (19) as explained further below. For the calculation of all the material defor-

mation quantities of interest, we follow for each fluid particle (sample path), a triplet of line elements that are initially orthogonal.

A. Generation of velocity-gradient sample paths

The φ^* equation is solved by the method outlined by Pope,[10] which is both efficient and accurate. Equation (19) for velocity gradients is marched in time using a predictor–corrector scheme similar to the second-order Runge–Kutta scheme (see Appendix D for details). At the end of predictor and corrector steps the velocity gradients are renormalized to make $(h_{ij}h_{ij})$ consistent with φ^* computed from Eq. (11). This renormalization is necessary to remove small inconsistencies resulting from truncation error. However, it is found that for the time step used ($\approx 0.1\tau_\eta$), very little renormalization is necessary. The velocity gradients of an ensemble of fluid particles at steady state in the simulations of Yeung *et al.*[20] provide the initial conditions for generating sample paths.

B. Computation of material element deformation quantities

Once the velocity-gradient time series is available, the following procedure is used to calculate the deformation quantities. Referring to Monin and Yaglom[12] (Sec. 24.5) the tensor $\mathbf{U}$ defined by

$$\frac{d}{dt}\mathbf{U} = \mathbf{h}\mathbf{U}, \tag{22}$$

with initial condition $\mathbf{U}(0) = \mathbf{J}$, contains all of the information on the deformation of infinitesimal material elements. Incompressibility demands that the determinant of $\mathbf{U}$ be unity. In the numerical procedure, the satisfaction of this condition requires that $\mathbf{U}$ be updated very accurately, which we achieve using a fourth-order Runge–Kutta scheme (see Appendix D).

Once $\mathbf{U}$ is known, the length and orientation (at any time t) of an infinitesimal material element that is initially $\mathbf{l}^\alpha(0)$, can be calculated from

$$\mathbf{l}^\alpha(t) = \mathbf{U}(t)\cdot\mathbf{l}^\alpha(0), \tag{23}$$

where

$$|\mathbf{l}^\alpha(0)| = 1, \quad \mathbf{l}^\alpha\cdot\mathbf{l}^\beta = \delta_{\alpha\beta}, \quad \text{for } \alpha,\beta = 1,3.$$

Knowing the orientations of all the material line elements of a triplet we use Eqs. (21) to compute all the quantities of interest.

The velocity gradient data from the FTS of Yeung *et al.*[20] is processed similarly.

VI. RESULTS AND DISCUSSION

In this section we first compare the one-time statistics of the model with that of the FTS data for $R_\lambda = 38$ data of Yeung *et al.*[20] To understand the importance of the L_{ij} terms in our model [Eq. (19)] we also include in our comparison the statistics generated by two simpler diffusion models of velocity derivatives. Next, we compare the statistics of material-element deformation calculated from our full model with those values calculated from the FTS. We then compare some of the two-time cross-covariances of the model time series with those of FTS. Finally we discuss the dependence of these quantities on Reynolds number.

A. Comparison of one-time statistics

The two simple models considered, T1 and T2, satisfy the kinematic constraints and yield consistent behavior of pseudodissipation. Model T1 is defined by

$$dh_{ij} = -h_{ij}(\tfrac{1}{2}\hat{a}^2 + \ln\varphi^*/2\tau)dt + D_{ijkl}\,dW_{kl}. \tag{24}$$

It contains only those terms needed to make the pseudodissipation a lognormal process. Model T2 is more sophisticated and includes the nonlinear term N_{ij}. There is also an additional term that is necessary to maintain the lognormality of pseudodissipation. Model T2 is given by

$$dh_{ij} = \left[-\left(N_{ij} - h_{ij}\frac{h_{lm}N_{lm}}{\varphi^*}\right) - h_{ij}\left(\frac{7}{2}\hat{a}^2 + \frac{\ln\varphi^*}{2\tau}\right)\right]dt + D_{ijkl}\,dW_{kl}. \tag{25}$$

In Table II the means (for the sake of brevity we use the term *mean* instead of the more accurate term *ensemble average*) of some important invariants of $\mathbf{h}$, calculated from the full model [Eq. (19)], model T1, and model T2 are compared with FTS values. The values of all of the invariant means obtained from the full model compare quite favorably with that of FTS. On the other hand, the values of the basic invariant means $\langle \mathrm{I}\rangle$ and $\langle \mathrm{III}\rangle$ obtained from the models T1 and T2 are quite wrong. This implies that even the homogeneity condition is not satisfied closely. Not surprisingly, the performance of model T2 is superior to that of model T1. But still model T2 is not even second-order consistent. So it is clear that the L_{ij} terms play an important role in making the model fourth-order consistent.

In Tables III and IV one-time statistics of the model and FTS are compared for various Reynolds numbers. Table III contains the means of the basic invariants (note that the velocity gradients are already normalized by τ_η) whereas in Table IV the means of locally normalized quantities [e.g., $\langle \mathrm{IV}/(\sqrt{\mathrm{I}}\,\mathrm{III})\rangle$] are presented. The agreement is uniformly good and by no means inevitable. As mentioned in Appendix B, only I, II, ln III, and k_1 are involved in constraining the model. Some of the other invariants (IV and V) are used to modify the coefficients slightly to further improve agreement. From the one-time statistics of the diffusion model T2,

TABLE II. Comparison of one-time statistics from various models.

Means of	FTS	Full model	Model T2	Model T1
I	0.498	0.527	0.638	0.622
III	0.511	0.475	0.363	0.385
II	−0.113	−0.128	−0.179	−0.006
IV	0.0401	0.0331	0.019	0.001
V	−0.158	−0.163	−0.134	−0.130
ln I	−1.07	−1.05	−0.900	−0.911
ln III	−1.35	−1.36	−1.62	−1.55
IV/√IIII	0.0737	0.0709	0.047	0.003
tr srsr/I III	0.263	0.265	0.212	0.170
ln III	−0.381	−0.382	−0.356	−0.335

TABLE III. Reynolds-number dependence of basic invariants (normalized by τ_η).

	$Re_\lambda = 38$		$Re_\lambda = 63$		$Re_\lambda = 93$	
Means of	FTS	Model	FTS	Model	FTS	Model
I	0.498	0.527	0.497	0.529	0.505	0.505
III	0.511	0.475	0.498	0.497	0.495	0.497
II	−0.113	−0.128	−0.110	−0.129	−0.117	−0.126
IV	0.0401	0.0331	0.0369	0.0371	0.0376	0.0396
V	−0.158	−0.163	−0.178	−0.187	−0.196	−0.202
ln I	−1.07	−1.05	−1.10	−1.14	−1.14	−1.18
ln III	−1.35	−1.36	−1.46	−1.46	−1.57	−1.50

it can be inferred that the L_{ij} terms play an important role in correctly determining all of the mean invariants in Table II. So it is not inevitable that the constants obtained from constraining I, II, ln III, and k_1 should, with only minor modifications also satisfy IV and V, not to mention the other statistics in Tables III and IV unless these L_{ij} terms capture some of the underlying physics.

In Table V we present means of $\langle \cos^2 \beta_p \rangle$, $\langle \cos^2 \beta_i \rangle$, and $\langle \cos^2 \beta_n \rangle$, where β_p, β_i, and β_n are the angles between the vorticity vector and the a_1, a_2, and a_3 strain-rate axes. The agreement is excellent.

B. Comparison of material-element deformation and two-time statistics

In this subsection the comparisons between the full model and FTS involve multitime behavior of the time series of **h**. Since no multitime constraint (except that the pseudo-dissipation be lognormal) was used in constructing the model, these tests are completely independent of the model building procedure. All the comparisons made in this subsection are for the $R_\lambda = 38$ case.

In Fig. 2, we compare the temporal evolutions of the mean of $\ln l$ and $\ln A$. In Fig. 3 we present the mean and variance of the rates of change of $\ln l$ and $\ln A$. Again the agreement between the model and FTS data is good. The zero values at time $t = 0$ in Fig. 3 is due to the fact that the material elements are initially oriented randomly with respect to principal strain directions resulting in no net rate of change.

TABLE V. Reynolds number dependence of β_p, β_i, and β_n.

	$Re_\lambda = 38$		$Re_\lambda = 63$		$Re_\lambda = 93$	
Quantity	FTS	Model	FTS	Model	FTS	Model
$\langle \cos \beta_p \rangle$	0.323	0.311	0.308	0.302	0.305	0.297
$\langle \cos \beta_i \rangle$	0.508	0.509	0.533	0.521	0.540	0.528
$\langle \cos \beta_n \rangle$	0.169	0.179	0.159	0.177	0.154	0.175

The asymptotic growth rates of $\langle \ln l \rangle$ and $\langle \ln A \rangle$ are, according to FTS data, $0.13/\tau_\eta$ and $0.16\ \tau_\eta$, respectively. Arguing that a material line element tends to align itself along the maximum positive strain-rate axis (a_1), and a material area element lies on the plane of maximum positive strain-rate and intermediate strain-rate (a_2) axes, Monin and Yaglom[12] (Sec. 24.5) estimate the growth rates to be approximately $\langle a_1 \rangle/\tau_\eta$ and $\langle a_1 + a_2 \rangle/\tau_\eta$, respectively. From FTS data $\langle a_1 \rangle/\tau_\eta$ and $\langle a_1 + a_2 \rangle/\tau_\eta$ are approximately 0.4 and 0.5, indicating that the estimates are high by a factor of 2.5. To understand the discrepancy we look at the premise of the argument. In Fig. 4 the mean of the angle between the maximum positive strain-rate direction and various line elements (which were initially randomly oriented with the a_1 direction) is presented as a function of time. If the material lines are in close alignment with the a_1 principal axis the angle would be zero: from Fig. 4 it is clear that the lines are far from being aligned with the a_1 direction.The reasons for this behavior are explored in detail by Girimaji and Pope.[3]

We now look at the behavior of the angles θ and α. Since the sign of the direction of the material lines are arbitrary, we deal with the absolute values of the angles. The statistics of the evolution of $\ln \sin|\theta|$ and $\ln \cos|\alpha|$ are completely determined by the statistics of the growth rate of $\ln l$ and $\ln A$. For, referring to Eqs. (21), we have

$$\ln \sin|\theta| = \ln A - \ln l_1 - \ln l_2.$$

Taking means and recognizing that l_1 and l_2 are statistically equivalent we have

TABLE IV. Reynolds-number dependence of one-time correlation.

	$Re_\lambda = 38$		$Re_\lambda = 63$		$Re_\lambda = 93$	
Means of	FTS	Model	FTS	Model	FTS	Model
I/φ^*	0.550	0.555	0.554	0.556	0.562	0.557
III/φ^*	0.450	0.445	0.446	0.444	0.438	0.443
$II/I^{1.5}$	−0.158	−0.184	−0.154	−0.184	−0.151	−0.187
$IV/\sqrt{I}$ III	0.0737	0.0709	0.0723	0.0712	0.0752	0.0694
srsr/I III	0.263	0.265	0.268	0.279	0.277	0.271
V/I III	−0.381	−0.382	−0.384	−0.397	−0.388	−0.385
$\ln(I/\varphi^*)$	−0.730	−0.700	−0.713	−0.697	−0.694	−0.695
$\ln(III/\varphi^*)$	−1.03	−1.00	−1.05	−1.00	−1.08	−1.01
$[\ln(I/\varphi^*)]^2$	0.867	0.764	0.840	0.755	0.816	0.751
$[\ln(III/\varphi^*)]^2$	1.72	1.55	1.81	1.55	1.93	1.57

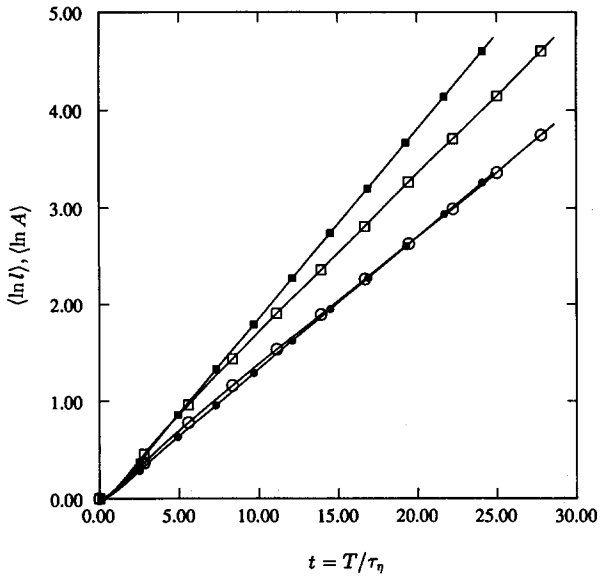

FIG. 2. Temporal evolution of material deformation quantities: O, $\langle \ln l \rangle$; □, $\langle \ln A \rangle$. The filled symbols represent the corresponding model quantities.

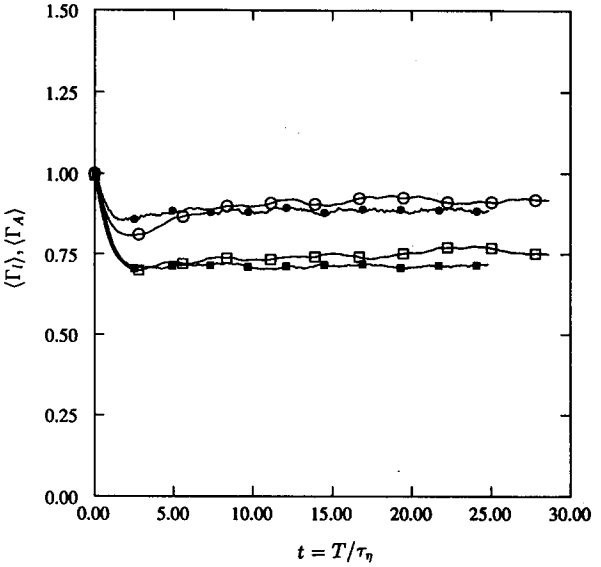

FIG. 4. Temporal evolution of the mean of the angles: (O) angle between the a_1 direction and l; and the (□) angle between a_3 direction and N of FTS data. The filled symbols represent the corresponding model quantities.

$$\frac{d}{dt}\langle \ln \sin|\theta| \rangle = \frac{d}{dt}\langle \ln A \rangle - 2\frac{d}{dt}\langle \ln l \rangle. \tag{26}$$

Similarly, for α, we obtain

$$\frac{d}{dt}\langle \ln \cos|\alpha| \rangle = -\left(\frac{d}{dt}\langle \ln A \rangle + \frac{d}{dt}\langle \ln l \rangle\right). \tag{27}$$

The values of the growth rates of $\langle \ln \sin|\theta| \rangle$ and $\langle \ln \cos|\alpha| \rangle$ calculated from the model and FTS data are tabulated in Table VI. The agreement is good to within about 25%.

The evolution of the means of the logarithm of the eigenvalues ($\ln w_1 \geqslant \ln w_2 \geqslant \ln w_3$) of the Cauchy–Green tensor are presented in Fig. 5: the agreement with the FTS results is again good. The logarithm of the intermediate value is positive, a fact that is consistent with $\langle a_2 \rangle$ being positive.

In Figs. 6–8 the cross-covariances of various quantities are compared. The correlations $\langle s_{12}(t)s_{12}(t+t') \rangle$ and $\langle \ln \mathrm{I}(t) \ln \mathrm{I}(t+t') \rangle$ show good agreement. The comparisons of $\langle r_{12}(t)r_{12}(t+t') \rangle$ and $\langle \ln \mathrm{III}(t) \ln \mathrm{III}(t+t') \rangle$ with corresponding FTS covariances show that the agreement is not good for the former but satisfactory for the latter. The behavior of the model $\langle r_{12}(t)r_{12}(t+t') \rangle$ for small t is understandably poor (owing to the nondifferentiability of the model time series). The poor correlation at large times indicates a certain lack of embodiment of physics in the model. The covariance $\langle \ln \mathrm{I}(t) \ln \mathrm{III}(t+t') \rangle$ is qualitatively correct though uniformly slightly overpredicted by the model. The covariance of $\langle \mathrm{I}(t)\mathrm{III}(t') \rangle$ is generally small and the model captures the poor correlation.

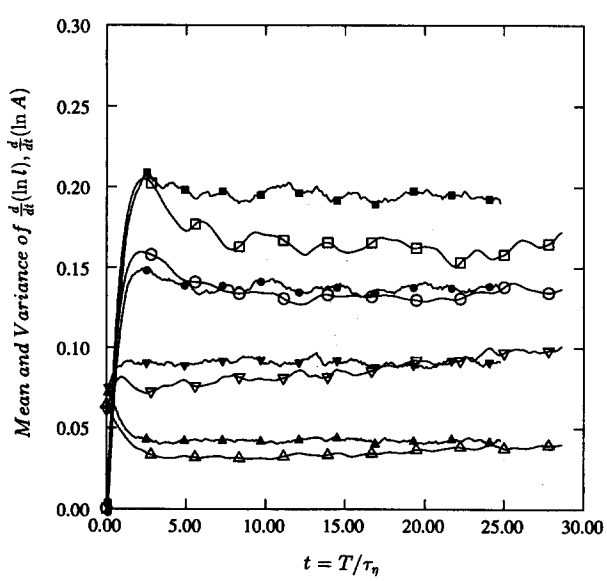

FIG. 3. Mean and variance of growth rates: O, $\langle \ln l \rangle$; □, $\langle \ln A \rangle$; △, var ln l; ▽, var ln A of FTS data. The filled symbols represent the corresponding model quantities.

C. Reynolds number dependence

We present the means of the basic invariants (globally normalized with τ_η) in Table III, invariants normalized lo-

TABLE VI. Reynolds number dependence of material element growth rates.

Growth rates of	$\mathrm{Re}_\lambda = 38$		$\mathrm{Re}_\lambda = 63$		$\mathrm{Re}_\lambda = 93$	
	FTS	Model	FTS	Model	FTS	Model
$\langle \ln l \rangle$	0.133	0.137	0.130	0.132	0.142	0.128
$\langle \ln A \rangle$	0.162	0.194	0.160	0.189	0.179	0.182
$\langle \ln \sin\|\theta\| \rangle$	−0.104	−0.080	−0.100	−0.075	−0.105	−0.074
$\langle \ln \cos\|\alpha\| \rangle$	−0.295	−0.331	−0.290	−0.321	−0.321	−0.310

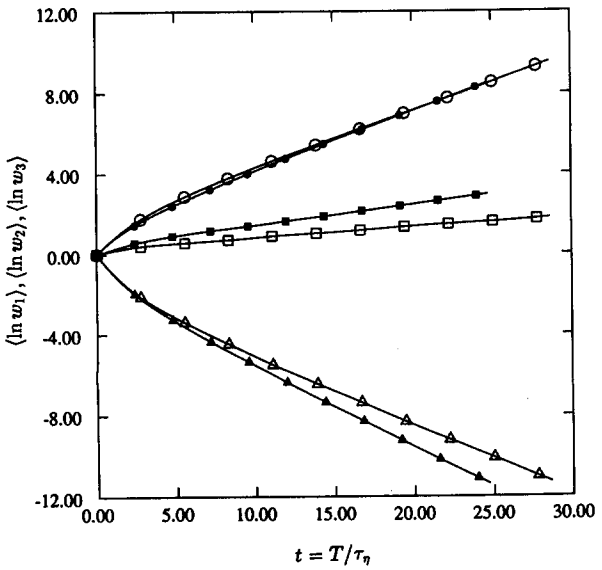

FIG. 5. Temporal evolution of eigenvalues of Cauchy–Green tensors $\omega_1(\bigcirc)$, $\omega_2(\square)$, and $\omega_3(\triangle)$ of FTS data. The filled symbols represent the corresponding model quantities.

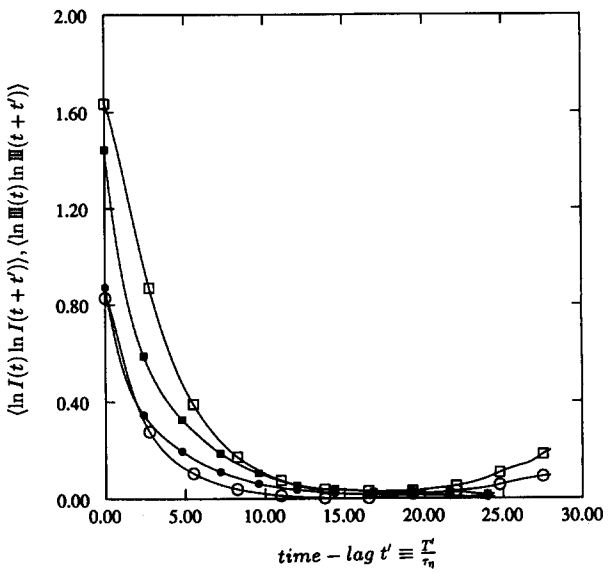

FIG. 7. Autocovariance of $\langle \ln \mathrm{I}(t) \ln \mathrm{I}(t+t') \rangle (\bigcirc)$ and $\langle \ln \mathrm{III}(t) \ln \mathrm{III}(t+t') \rangle (\square)$ of the FTS data. The filled symbols represent the corresponding model quantities.

cally in Table IV and, asymptotic mean growth rates of material elements in Table VI, for three different Reynolds numbers. The contents of the tables can be summarized as follows.

(1) The means of basic invariants show some variation with Reynolds numbers. Except for V and ln III, the variation is small and shows no trend. The increase of ln III with Reynolds number is quantified by Yeung and Pope[14] and the model appears to capture this trend to a certain extent.

(2) Of the locally normalized quantities $\langle \mathrm{IV}/(\sqrt{\mathrm{I}}\,\mathrm{III}) \rangle$, $\langle \mathrm{V}/(\mathrm{I}\,\mathrm{III}) \rangle$, and $\langle \mathrm{tr}(\mathbf{s}^+\mathbf{r}^+\mathbf{s}^+\mathbf{r}^+)/(\mathrm{I}\,\mathrm{III}) \rangle$ show little or no variation with Reynolds number. The mean of $[\ln(I/\varphi^*)]^2$ decreases slightly and that of $[\ln(\mathrm{III}/\varphi^*)]^2$ increases with Reynolds number. The model does not capture these trends too well. With other quantities the variation is too little to infer a trend and the performance of the model is good.

(3) The material deformation rates appear Reynolds number independent. The asymptotic rates are probably completely determined by the one-time correlations, with the

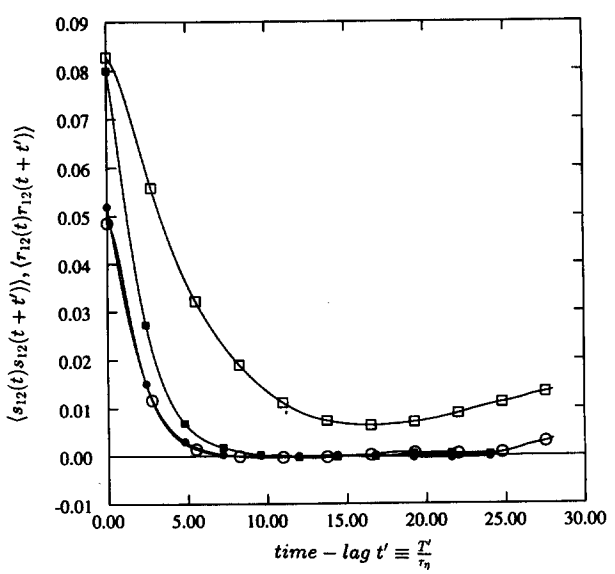

FIG. 6. Autocovariance of $\langle s_{12}(t) s_{12}(t+t') \rangle (\bigcirc)$ and $\langle r_{12}(t) r_{12}(t+t') \rangle (\square)$ of the FTS data. The filled symbols represent the corresponding model quantities.

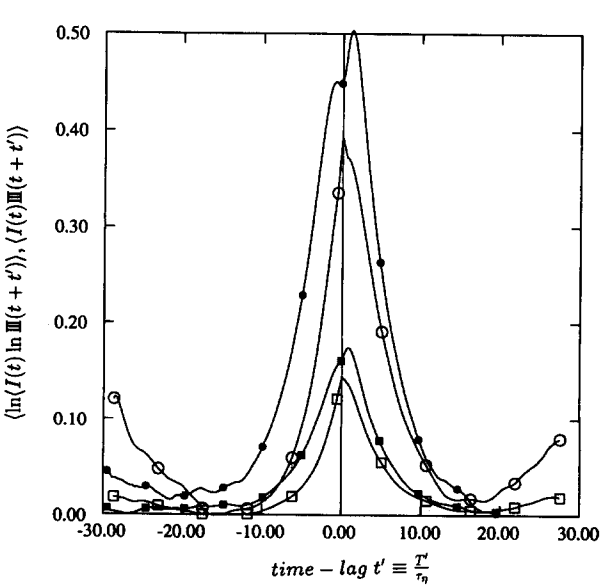

FIG. 8. Cross-covariance of $\langle \ln \mathrm{I}(t) \ln \mathrm{III}(t+t') \rangle (\bigcirc)$ and $\langle \mathrm{I}(t) \mathrm{III}(t+t') \rangle (\square)$ of the FTS data. The filled symbols represent the corresponding model quantities.

absolute magnitudes of strain and vorticity determining only the time taken to achieve the asymptotic values. The performance of the model is qualitatively good but the asymptotic growth rate of area is overestimated by about 20% for the worst case.

The Reynolds number dependence of enstrophy and dissipation correlations are presented in Yeung and Pope.[14] The model covariances do not vary much with Reynolds number because of the fact that the terms containing $\hat{a}$ and $1/\tau$ are much smaller than the other terms in the equations.

VII. SUMMARY AND CONCLUSION

In this paper we first established that the velocity gradients following fluid particles are amenable to being modeled by a diffusion process (Sec. III). We then developed a diffusion model for normalized velocity gradients ($\mathbf{h}$) following fluid particles. For homogeneous, isotropic turbulence the normalized velocity gradients are given by Eq. (19). For the case of inhomogeneous flows the unnormalized velocity gradients are more useful and their increments are given by Eq. (20).

The conclusions regarding the model are the following.

(1) The model has a fairly simple form, with only four numerically determined constants. It produces continuous Markovian sample paths that are, however, not differentiable. Its main asset is its computational simplicity.

(2) Its performance for one-time statistics (both constrained and unconstrained moments) is quite good.

(3) Its performance for material element deformation is qualitatively good but quantitatively not quite accurate. The material line and surface element growth rates are underpredicted by 20%, which, however, is a small discrepancy considering that the previous estimates (see Sec. V) overpredicted the rates by 250%.

(4) The two-time strain-rate statistics agree well with FTS data. The two-time vorticity-component correlation is poorly reproduced, and the covariance of enstrophy is fair. There is perhaps some physics that is not embodied in the model. The two-time dissipation-enstrophy cross-covariances are correct to within about 20%.

(5) Although the model was developed for moderate Reynolds numbers, we conjecture, based on the Reynolds-number dependence study in Sec. VI, that the model can be used for higher Reynolds numbers and for inhomogeneous nonstationary flows.

Based on the above assessment, we feel that the model will be useful for the study of material elements in turbulence, especially for the investigation of surface elements as in the work of Pope and Cheng.[4]

ACKNOWLEDGMENTS

This work was supported by U.S. Air Force Office of Scientific Research (Grant No. AFOSR-88-0052), and in part by the U.S. Department of Energy (Contract No. DE-ACS 03-83ER 13038). This research was conducted using the Cornell National Computing Facility, a resource of the Center for Theory and Simulations in Science and Engineering (Cornell Theory Center), which receives major funding from the National Science Foundation and the IBM Corporation, with additional support from New York State and Members of the Corporate Research Institute.

APPENDIX A: DETERMINATION OF M AND D

In this appendix we derive expressions for the drift term $\mathbf{M}$ and the diffusion term $\mathbf{D}$ so that the process implied by the velocity gradient model, Eq. (7), for pseudodissipation is lognormal.

For Eq. (11) to be equivalent to Eq. (12) we just require that the conditional means and variances of these equations be the same to first order (Karlin and Taylor,[16] p. 159). This condition yields the following constraint equations for M_{ij} and D_{ijkl}:

$$2h_{ij}(M_{ij} - N_{ij}) + D_{ijkl}D_{ijkl} = \varphi^*(\hat{a}^2 - \ln \varphi^*/\tau) \tag{A1}$$

and

$$\langle d_{kl}d_{kl}|\varphi^* = \phi\rangle = \langle \hat{a}^2\varphi^{*2}|\varphi^* = \phi\rangle = \hat{a}^2\phi^2, \tag{A2}$$

where

$$d_{kl} = h_{ij}D_{ijkl},$$

and ϕ is the state-space variable of φ^*.

To determine a $\mathbf{D}$ that satisfies Eq. (A2) we considered two models: an isotropic model

$$D_{ijkl} = b_1\delta_{ij}\delta_{kl} + b_2\delta_{ik}\delta_{jl} + b_3\delta_{il}\delta_{jk}, \tag{A3}$$

where b_1, b_2, and b_3 are constants; and, a general linear model containing six additional terms linear in $\mathbf{h}$. It is found that the isotropic model performs better in a detailed comparison with FTS (described further below).

Proceeding with the isotropic model to determine the constants, d_{kl} is given by

$$d_{kl} = h_{ij}(b_1\delta_{ij}\delta_{kl} + b_2\delta_{ik}\delta_{jl} + b_3\delta_{il}\delta_{jk}) = b_2h_{kl} + b_3h_{lk}. \tag{A4}$$

Hence the conditional mean in Eq. (A2) is

$$\langle d_{kl}d_{kl}|\varphi^* = \phi\rangle = (b_2^2 + b_3^2)\phi + 2\langle b_2b_3h_{kl}h_{lk}|\varphi^* = \phi\rangle.$$

This means that if either b_2 or b_3 is zero, Eq. (A2) is satisfied. The choice is arbitrary: we take $b_3 = 0$, leading to $b_2 = \hat{a}\sqrt{\varphi^*}$. The incompressibility condition requires $D_{iikl} = 0$, leading to

$$3b_1 + b_2 + b_3 = 0. \tag{A5}$$

Hence with the values of b_2 and b_3 already obtained, we have

$$b_1 = -\tfrac{1}{3}\hat{a}\sqrt{\varphi^*}.$$

So the model for $\mathbf{D}$ is given by

$$D_{ijkl} = \hat{a}\sqrt{\varphi^*}(\delta_{ik}\delta_{jl} - \tfrac{1}{3}\delta_{ij}\delta_{kl}). \tag{A6}$$

Referring to Eq. (A6) the diffusion term yields the increment

$$dh_{ij}^d = D_{ijkl}\,dW_{kl} = \hat{a}\sqrt{\varphi^*}(dW_{ij} - \tfrac{1}{3}dW_{pp}\,\delta_{ij}),$$

whereas the more complicated linear model [after imposing incompressibility and Eq. (A2) constraints] yields

$$dh_{ij}^{d} = q h_{ij}\, dW_{pp} + \hat{a}\sqrt{\varphi^*}(dW_{ij} - \tfrac{1}{3} dW_{pp}\,\delta_{ij}),$$

where q is a constant. Thus the difference between the isotropic model and linear model is the extent of correlation between h_{ij} and dh_{ij}. Calculations from FTS data show that h_{ij} and dh_{ij} are almost uncorrelated, consistent with zero value for q, thus ratifying the isotropic model.

From Eq. (A6) we obtain

$$D_{ijkl}D_{ijkl} = \hat{a}^2\varphi^*(\delta_{ii}\delta_{jj} + \tfrac{1}{3}\delta_{ii}\delta_{jj} - \tfrac{2}{3}\delta_{ik}\delta_{jl}\delta_{ij}\delta_{kl}) = 8\hat{a}^2\varphi^*. \tag{A7}$$

Incorporating Eq. (34) in Eq. (28) leads to the constraint on M,

$$h_{ij}(M_{ij} - N_{ij}) = -\varphi^*(\tfrac{7}{2}\hat{a}^2 + \ln\varphi^*/2\tau).$$

Clearly, M defined as

$$M_{ij} = -h_{ij}\left(\frac{7}{2}\hat{a}^2 + \frac{\ln\varphi^*}{2\tau} - \frac{h_{lm}N_{lm}}{\varphi^*}\right) + L_{ij}, \tag{A8}$$

where L is an isotropic tensor function of h such that

$$h_{ij}L_{ij} = 0, \quad L_{ii} = 0, \tag{A9}$$

satisfies Eq. (A1) as well as incompressibility and isotropy conditions.

APPENDIX B: DETERMINATION OF C USING CONSTRAINT EQUATIONS

In this appendix we develop a method of determining coefficients C in Eq. (18) that cause the model to yield specified values of the moments.

First, starting from Eq. (16), the evolution equations for ensemble averages of invariants are derived. The equations for the invariants considered are [for convenience we drop superscript + and define $k_1 \equiv \mathrm{IV}/(\sqrt{\mathrm{I}}\,\mathrm{III})$ and $k_2 \equiv s_{ij}r_{jk}s_{kl}r_{li}/(\mathrm{I\,III})$],

$$\frac{d}{dt}\langle \mathrm{I}\rangle = \left\langle -7\hat{a}^2\mathrm{I} - \mathrm{I}\frac{\ln\varphi^*}{\tau} + 5\hat{a}^2\varphi^* + 2s_{ij}L_{ij}\right\rangle, \tag{B1}$$

$$\frac{d}{dt}\langle \mathrm{II}\rangle = \left\langle -7\hat{a}^2\mathrm{II} - \mathrm{II}\frac{\ln\varphi^*}{\tau} + 3s_{ij}s_{jk}s_{ki}\right\rangle, \tag{B2}$$

$$\frac{d}{dt}\langle \mathrm{IV}\rangle = \left\langle -\frac{21}{2}\hat{a}^2\mathrm{IV} - 3\mathrm{II}\frac{\ln\varphi^*}{3\tau} + L_{ij}r_{jk}r_{ki} + s_{ij}L_{jk}r_{ki} + + s_{ij}r_{jk}L_{ki}\right\rangle, \tag{B3}$$

$$\frac{d}{dt}\langle \mathrm{V}\rangle = \left\langle -14\hat{a}^2 V - 2V\frac{\ln\varphi^*}{\tau} + L_{ij}s_{jk}r_{kl}r_{li} + s_{ij}L_{jk}r_{kl}r_{li} + s_{ij}s_{jk}L_{kl}r_{li} + s_{ij}s_{jk}r_{kl}L_{li}\right\rangle, \tag{B4}$$

$$\frac{d}{dt}\langle \ln \mathrm{I}\rangle = \left\langle -7\hat{a}^2 - \frac{\ln\varphi^*}{\tau} + 3\hat{a}^2\varphi^*/\mathrm{I} + 2s_{ij}L_{ij}/\mathrm{I}\right\rangle, \tag{B5}$$

$$\frac{d}{dt}\langle \ln \mathrm{III}\rangle = \left\langle -7\hat{a}^2 - \frac{\ln\varphi^*}{\tau} + \hat{a}^2\varphi^*/\mathrm{I} + 2r_{ij}L_{ij}/\mathrm{I}\right\rangle, \tag{B6}$$

$$\frac{d}{dt}\langle k_1\rangle = \left\langle \left[-k_1\left(\sqrt{\mathrm{I}}(3\hat{a}^2\varphi^* + 2r_{ij}L_{ij}) - \frac{\mathrm{III}}{\sqrt{\mathrm{I}}}(2\hat{a}^2\varphi^* + s_{ij}L_{ij})\right) + L_{ij}r_{jk}r_{ki} + s_{ij}L_{jk}r_{ki} + s_{ij}r_{jk}L_{ki}\right] (\sqrt{\mathrm{I}}\,\mathrm{III})\right\rangle, \tag{B7}$$

$$\frac{d}{dt}\langle k_2\rangle = \langle\{ -2k_2(\mathrm{III}\,L_{ij}s_{ij} + \mathrm{I}\,L_{ij}r_{ij}) + \hat{a}^2\varphi^*[\mathrm{III}(\tfrac{5}{6} - 5k_2) + \mathrm{I}(\tfrac{1}{2} + 3k_2)] + L_{ij}r_{jk}s_{kl}r_{li} + s_{ij}L_{jk}s_{kl}r_{li} + s_{ij}r_{jk}L_{kl}r_{li} + s_{ij}r_{jk}s_{kl}L_{li}\}/(\mathrm{I\,III})\rangle. \tag{B8}$$

If we start the calculations with a guess of L_{ij} and an ensemble of particles with arbitrarily specified initial velocity gradients, the means of the invariants evolve to a steady state according to the above equations. If our choice of L_{ij} is good, the steady-state values of the invariant means match the specified values. On the other hand, even if the moments of the initial distribution of the velocity gradients are as required, an incorrect choice of L_{ij} leads to steady-state moments that are quite wrong. So it is clear how the L_{ij} terms on the right-hand side of the above equations influence the steady-state values of the invariant means.

The practical purpose of the above equations is twofold. They help identify scalar functions that are important and thus help in making a good choice $\{\Gamma\}$. More importantly, once a choice of $\{\Gamma\}$ has been made these equations can be used to determine C, and that procedure is now described.

The evolution equations Eqs. (B1)–(B8) of the invariant means can be written in the general form [referring to Eq. (18) for the form of L],

$$\frac{d}{dt}y_\alpha = K_\alpha + \sum_{\beta=1}^{\Lambda}\sum_{\lambda=1}^{11} C_{\beta\lambda}\,\Gamma_\beta\, Q_{\alpha\lambda}, \tag{B9}$$

where $Q_{\alpha\lambda}$ is composed of invariants such as $\langle s_{ij}r_{jk}X_{kl}\rangle$; K_α is defined by Eqs. (B1)–(B8) and includes the Q-type terms arising from $\mathbf{X}^3$, $\mathbf{X}^4$, and $\mathbf{X}^{10}$ of L; $\mathbf{y} \equiv \{y_1, y_2, \ldots, y_N\}$ are the N invariants we want to constrain; and Λ is the number of scalar functions. It may now be seen how C influences the evolution and ultimately the steady-state values of the mean invariants.

In vector form Eq. (B9) is

$$\frac{d}{dt}\mathbf{y} = \mathbf{K} + \mathbf{Q}\mathbf{c}, \tag{B10}$$

where $\mathbf{c} = \Gamma\mathbf{C}$. If we start with a velocity gradient ensemble that has the desired moments, C can be calculated from the above equation by knowing K, Q, and Γ and setting the left-hand side to zero. If this C is used in Eq. (16) to update h, it is likely that the new values of Q (which involve higher-order moments than those constrained) are different than those in the initial step, leading to a new C. Using the new C, we can again update the velocity gradients and continue the iterations until C converges; but there is no reason to suppose that this scheme converges, and if it does, it may not converge to the correct moment values. A certain convergence to the correct moment values can be obtained if the following procedure is used to calculate c.

The invariants y adopt the required values $\mathbf{y}^*$, if y evolves by

$$\frac{d}{dt}\mathbf{y} = -\mathbf{R}(\mathbf{y}-\mathbf{y}^*), \tag{B11}$$

where R is any positive definite, symmetric matrix. For then we have

$$\frac{d}{dt}|\mathbf{y}-\mathbf{y}^*|^2 = -2(\mathbf{y}-\mathbf{y}^*)^T\mathbf{R}(\mathbf{y}-\mathbf{y}^*) < 0. \tag{B12}$$

Comparing Eqs. (B10) and (B11) it may be seen that with c chosen according to

$$\mathbf{c} = -\mathbf{Q}^{-1}[\mathbf{K}+\mathbf{R}(\mathbf{y}-\mathbf{y}^*)], \tag{B13}$$

y evolves according to both Eqs. (B10) and (B11). At large times y asymptotes to $\mathbf{y}^*$, and hence c converges, say, to $\mathbf{c}^*$. Then y generated by using $\mathbf{c}^*$ will take the desired values $\mathbf{y}^*$.

The obvious choice of R in Eq. (B13) (which affects only the rate at which the stationary state is reached) is

$$\mathbf{R} = \mathbf{J}/T_s, \tag{B14}$$

where T_s is a specified time scale and J is the identity matrix.

In solving for C the number of constraints is N and the number of unknowns is Λ times the number of candidate tensors. As mentioned in Sec. IV C the only tensor functions considered are $\mathbf{X}^3$, $\mathbf{X}^4$, $\mathbf{X}^{10}$, and $\Lambda = 2$. For the sake of computational convenience we treat $p\mathbf{X}^3$, $p\mathbf{X}^4$, $p\mathbf{X}^{10}$, and $\mathbf{X}^3/p$, $\mathbf{X}^4/p$, and $\mathbf{X}^{10}/p$ as six different tensor functions. For then, we can treat Γ as having only one element, which is unity leading to $\mathbf{c} \equiv \mathbf{C}$. Thus the constants in the model can be obtained directly from Eq. (B13).

We use the singular value decomposition (SVD) method of solution to calculate c from Eq. (B13) for two reasons. First, if we have more or less constraints than unknowns the SVD yields a reasonable solution vector: a c that minimizes the mean-square difference $\{\mathbf{y}-\mathbf{y}^*\}$ for the former; and the shortest solution vector c that satisfies the constraints for the latter case. Second, if the system of constraint Eqs. (B1)–(B8) is overdetermined, numerical roundoff errors and statistical errors can lead to spurious solutions of Eq. (B3) with other methods.This difficulty can be circumvented with SVD by dropping from consideration the singular vectors corresponding to *small* singular values in computing the solution vector c (Ref. 21). In our calculations a singular value is deemed *small* if it is smaller than 1% of the largest value.

Any rejection of small singular values will lead to a $\mathbf{c}^*$ that minimizes the mean-square difference rather than exactly satisfy the constraints. Consequently some constraints are not as well satisfied as the others, requiring that we impose these constraints more stringently than the others. This is achieved by weighting the corresponding equations more heavily, thus increasing the contribution of this constraint to the mean-square difference. In our problem the weights are specified based on the initial value of K. Given that we start from FTS field, referring to Eq. (B10), the larger the value of a particular K_α initially, the faster is the deviation of y_α from the corresponding y_α^*. Hence that particular invariant would require a larger L participation to hold at the desired value. So the weights assigned to invariants are proportional to their corresponding initial K values.

Invariants I, II, ln III, and k_1 are the only ones used for determining C, since it is found that this C yields close to required values for the other mean invariants. The constraints imposed by the invariants IV and V are used only to fine tune C to further reduce the mean-square difference between the model and the desired values.

The above strategy is implemented as follows. A choice of the scalar functions Γ is made. A large number (10 000) of sample fluid particles are considered with their initial velocity gradient distribution taken from a stationary FTS ensemble: hence $\mathbf{y}(0) = \mathbf{y}^*$. From this distribution the initial values of Q and K are obtained. The solution vector c is then computed from Eq. (B13) using singular-value decomposition to give a first guess of L. A simulation over one time step is then performed using Eq. (16) to compute the new velocity gradients. New values of c are then computed with new values of invariants. Such iterations are carried out until consecutive steps yielded almost identical c values.

APPENDIX C: REALIZABILITY OF THE MODEL

This appendix establishes the fact that the proposed model does not violate the realizability requirements, i.e., that pseudodissipation, dissipation, and enstrophy are bounded above, and do not become negative; and that the diffusion process for h_{ij} leads to bounded values.

Since $\ln \varphi^*$ is a Gaussian process, φ^* does not become negative and is bounded above in probability;

$$\lim_{\phi \to \infty} \Pr\{\varphi^* > \phi\} = 0.$$

The velocity gradient h_{ij} is also bounded in probability since for each component

$$|h_{ij}| \leqslant \sqrt{\varphi^*}.$$

The L terms only reorient the h tensor [referring to Eq. (15)] without affecting the magnitude, and hence do not affect the realizability argument.

Note that I and III are calculated as sums of squares of h_{ij} (for which we carry well-behaved evolution equations), and hence cannot become negative. Moreover, since $\mathrm{I} + \mathrm{III} = \varphi^*$, both I and III are also bounded above. So the issue of realizability is reduced to the question, whether either I or III ever goes to zero, and if one of the two does, whether it will recover to positive values.

Case(i): Limit I→0. From Eq. (19), in this limit the increment in strain rate is given by

$$\begin{aligned} ds_{ij}^+ = &-(r_{ik}^+ r_{kj}^+ + \delta_{ij}\,\mathrm{III}/3) \\ &+ C_{24}\ln\varphi^*\sqrt{\mathrm{III}/\mathrm{I}}\,(r_{ik}^+ r_{kj}^+ - s_{ij}^+\,\mathrm{IV}/\varphi^* \\ &+ \delta_{ij}\,\mathrm{III}/3) + D_{ijkl}^s\,dW_{kl}, \end{aligned} \tag{C1}$$

where D_{ijkl}^s is the symmetric part of D. So as $\mathrm{I} \to 0$, $ds_{ij}^+ \to \pm\infty$, depending on the relative orientation of strain-rate axes and vorticity vector. Hence the strain rates change rapidly in this limit leading a rapid increase in dissipation. This implies that the model dissipation does not take very low values, which is also a characteristic of FTS dissipation.

Case (ii): Limit III→0. In this limit the evolution equation for rotation rate is given by

$$dr_{ij}^{+} = C_{13}\sqrt{\mathrm{I/III}}\,r_{ij}^{+}\,\mathrm{II}/\varphi^{*} + C_{1,10}\sqrt{\mathrm{I/III}}\,(s_{ik}^{+}r_{kj}^{+} + r_{ik}^{+}s_{kj}^{+}) + D^{r}_{ijkl}\,dW_{kl}, \tag{C2}$$

where D^{r}_{ijkl} is the antisymmetric part of **D**. In terms of vorticity vector (ω_i) the equation can be rewritten as

$$d\omega_k^{+} = C_{13}(\sqrt{2\mathrm{I}}\,\mathrm{II}/\varphi^{*})\omega_k^{+}/(\omega_p^{+}\omega_p^{+})^{1/2} + 2C_{1,10}\sqrt{2\,\mathrm{I}}s_{kp}^{+}\omega_p^{+}/(\omega_l^{+}\omega_l^{+})^{1/2} + e_{jki}D^{r}_{ijlm}\,dW_{lm}, \tag{C3}$$

where e_{kji} is the alternating tensor. The above equation can be further simplified by considering a coordinate system whose one-axis lies along the vorticity tensor. Then

$$d\omega_k^{+} = C_{13}(\sqrt{2\mathrm{I}}\,\mathrm{II}/\varphi^{*})\delta_{1k} + 2C_{1,10}\sqrt{2\mathrm{I}}s_{k1}^{+} + e_{kji}D^{r}_{ijlm}\,dW_{lm}. \tag{C4}$$

It is clear that in this limit $d\omega_k^{+}$ is nonzero, hence III will recover to positive values. The rate of change in this limit, however, is finite, indicating that III will recover slowly from small values, a fact that is consistent with FTS observations.

Thus, h_{ij} is bounded and the behavior of pseudodissipation, dissipation, and enstrophy in the limits of zero and infinity, is as required.

APPENDIX D: NUMERICAL ALGORITHMS

In this appendix the algorithms used for updating the velocity gradients and for computing the tensor **U** are discussed.

Given a time step Δt following Pope,[10] Δt_d and Δt_r are defined as follows:

$$\Delta t_d \equiv f(\Delta t)\tau, \tag{D1}$$

$$\Delta t_r \equiv \Delta t_d(1 - \Delta t_d/2\tau), \tag{D2}$$

where τ is as defined in Eq. (11) and

$$f(\Delta t) \equiv 1 - \exp(\Delta t/\tau) \approx \frac{[\Delta t/\tau + 0.31(\Delta t/\tau)^2]}{[1 + 0.81(\Delta t/\tau) + 0.31(\Delta t/\tau)^2]}.$$

Equation (5) is updated as follows:

$$\ln\varphi^{*}(t+\Delta t) = \ln\varphi^{*}(t) - \frac{1}{\tau}\left(\frac{\sigma^2}{2} + \ln\varphi^{*}\right)\Delta t_d + 2\frac{\hat{a}}{\sqrt{\varphi^{*}}}(h_{ij}\xi_{ij})\sqrt{\Delta t_r}, \tag{D3}$$

where the components of ξ are independent standardized Gaussian random variables so that

$$\langle\xi_{ij}\rangle = 0,$$

and,

$$\langle\xi_{ij}\xi_{kl}\rangle = \delta_{ik}\delta_{jl}.$$

The velocity gradients are updated using the following predictor and corrector equations:

$$h'_{ij} = h_{ij}(t) + M_{ij}(h,t)\Delta t_d + \hat{a}\sqrt{\varphi^{*}}, \times[\xi_{ij} - (\delta_{ij}/3)\xi_{kk}]\sqrt{\Delta t_r}, \tag{D4}$$

$$h_{ij}(t+\Delta t) = h_{ij}(t) + M_{ij}(h',t)\Delta t_d + \hat{a}\sqrt{\varphi^{*}} \times[\xi_{ij} - (\delta_{ij}/3)\xi_{kk}]\sqrt{\Delta t_r}. \tag{D5}$$

At the end of the predictor and the corrector steps the velocity gradients are normalized to be consistent with φ^{*}.

The tensor **U** is integrated using the fourth-order Runge–Kutta scheme. The intermediate steps involved are the Euler half-step predictor,

$$U_{ij}^{1}(t) = U_{ij}(t) + (\Delta t/2)h_{ik}(t)U_{kj}(t); \tag{D6}$$

the backward Euler corrector step,

$$U_{ij}^{2}(t) = U_{ij}(t) + (\Delta t/4)[h_{ik}(t) + h_{ik}(t+\Delta t)]U_{kj}^{1}(t); \tag{D7}$$

the midpoint predictor step,

$$U_{ij}^{3}(t) = U_{ij}(t) + (\Delta t/2)[h_{ik}(t) + h_{ik}(t+\Delta t)]U_{kj}^{2}(t); \tag{D8}$$

and the Simpson corrector step,

$$U_{ij}(t+\Delta t) = U_{ij}(t) + (\Delta t/6)[h_{ik}(t)U_{kj}(t) + \{h_{ik}(t) + h_{ik}(t+\Delta t)\}\{U_{kj}^{1} + U^{2}kj\} + h_{ik}(t+\Delta t)U_{kj}^{3}(t)]. \tag{D9}$$

This scheme is found to give the required degree of accuracy.

[1] G. K. Batchelor, Proc. R. Soc. London Ser. A **213**, 349 (1952).
[2] P. K. Yeung, S. S. Girimaji, and S. B. Pope, to appear in Combust. Flame.
[3] S. S. Girimaji and S. B. Pope, submitted to J. Fluid Mech.
[4] S. B. Pope and W. K. Cheng, *The Stochastic Flamelet Model For Turbulent Premixed Combustion*, Proceedings of the 22nd International Symposium on Combustion (The Combustion Institute, Pittsburgh, 1988), pp. 781–789.
[5] G. I. Taylor, Proc. London Math. Soc. Ser. B **20**, 196 (1921).
[6] P. A. Durbin, J. Fluid Mech. **100**, 279 (1980).
[7] J. D. Reid, Boundary Layer Meteorol. **16**, 3 (1979).
[8] D. C. Haworth and S. B. Pope, Phys. Fluids **29**, 387 (1986).
[9] S. B. Pope, Technical Report No.FDA-88-11, Sibley School of Mechanical and Aerospace Engineering, Cornell University, 1988.
[10] S. B. Pope, Technical Report No. FDA-88-07, Sibley School of Mechanical and Aerospace Engineering, Cornell University, 1988.
[11] W. T. Ashurst, A. R. Kerstein, R. M. Kerr, and C. H. Gibson, Phys. Fluids **30**, 2343 (1987).
[12] A. S. Monin and A. M. Yaglom, in *Statistical Fluid Mechanics*, edited by J. L. Lumley (MIT Press, Cambridge, 1975), Vol. 2.
[13] P. Vieillefosse, J. Phys. (Paris) **43**, 837 (1982).
[14] P. K. Yeung and S. B. Pope, J. Fluid Mech. **207**, 531 (1989).
[15] A. M. Obukhov, Adv. Geophys. **6**, 113 (1959).
[16] S. Karlin and H. M. Taylor, *A Second Course in Stochastic Processes* (Academic, New York, 1984).
[17] S. B. Pope, Prog. Energy Combust. Sci. **11**, 119 (1985).
[18] S. B. Pope, Phys. Fluids **30**, 2374 (1987).
[19] S. Pennisi and M. Trovato, Int. J. Eng. Sci. **25**, 1059 (1987).
[20] P. K. Yeung, S. S. Girimaji, and S. B. Pope Technical Report No. FDA-88-02, Sibley School of Mechanical and Aerospace Engineering, Cornell University, 1988.
[21] W. H. Press, B. P. Flannery, S. A. Teukolsky, and W. T. Vetterling, *Numerical Recipes: The Art of Scientific Computing* (Cambridge U. P., Cambridge, MA, 1987).